Ab initio simulations of sodium using time-dependent density-functional theory

Joachim Theilhaber*
Electronic Research Laboratory, University of California, Berkeley, California 94720
(Received 14 February 1992; revised manuscript received 31 July 1992)

A first-principles scheme for the dynamical simulation of matter based on time-dependent density-functional theory is presented and used for the prediction of the properties of bulk sodium. In contrast to the Car-Parrinello method, the scheme does not require the imposition of orthonormality constraints in the electronic equations of motion, resulting in algorithmic simplification. The execution times of the two methods are comparable. Difficulties associated with electron-ion equilibration in metallic systems are found to be a consequence of the suppression of spontaneous emission in the underlying quantum-classical model, and thus differ in fundamental nature from analogous numerical problems encountered in the Car-Parrinello method. The direct calculation of nonequilibrium electronic properties is presented as a remoter application of the scheme.

I. INTRODUCTION

In recent years schemes for the dynamical simulation of matter from first principles have been developed on the basis of the Car-Parrinello method,[1,2] in which electronic wave functions evolve according to artificial dynamics, in such a way as to adiabatically follow ion motion and provide a fully quantum-mechanical description of the forces mediated by the electrons. We present here an alternative approach which uses time-dependent density-functional (TDDF) theory[3] as a starting point, and introduces Schrödinger-like equations for the time evolution of the electronic wave functions.[4] The scheme is similar to those used by Fois *et al.*[5,6] and Kalia *et al.*,[7] but with a different emphasis: the authors of Refs. 5 and 7 have studied the behavior of one or a few electrons in nonmetallic systems, in simulations where the ion-ion interaction is overwhelmingly determined by a classical pair potential, which is not calculated on a first-principles basis. On the other hand, we aim for a fully self-consistent description of electron-ion motion.

Two advantages result from the TDDF approach: (1) if used for the adiabatic evolution of the electronic wave functions, as in the Car-Parrinello method, the TDDF scheme avoids explicit orthonormality constraints in the equations of motion, resulting in algorithmic simplification, and (2) because electron dynamics are now allowed, direct computation of at least some electronic transport properties becomes possible.[7] We present here results for the bulk properties of sodium at various temperatures, principally in the solid phase, using the TDDF scheme to achieve quasiadiabatic electron evolution, and with local pseudopotentials to model the ion cores. Results for the radial distribution functions, the velocity autocorrelation functions, the phonon spectrum, and the melting temperature are found to be in reasonable agreement with experiment, and comparable to those obtained using the Car-Parrinello method.[8] The computer times required to achieve these results also appear comparable. Equally accurate results for sodium in the liquid phase, including calculation of the self-diffusion coefficients, were presented in a previous paper,[9] where only the liquid state was considered.

The simulations of sodium under the TDDF scheme exhibit over time an irreversible transfer of energy from the ionic to the electronic degrees of freedom which if unchecked leads to physically meaningless results. While a similar process is observed in simulations using the Car-Parrinello method, and signals the breakdown of adiabaticity of the artificial electronic dynamics in response to ion motion, the origin of the phenomenon in the TDDF scheme is markedly different. It can be traced to the suppression of spontaneous emission in the system, a consequence of the "mixed" nature of the model, which combines classical ions with quantum-mechanical electrons.

In what follows, we present the algorithmic formulation of the TDDF scheme, the simulation results, and a discussion in some depth of the breakdown of adiabaticity and its relation to the quantum-classical model. While no new physical results are recovered from the present simulations of sodium, they provide a rigorous "test bed" for the TDDF approach in the context of a nontrivial application. We plan to strongly pursue other applications in the near future.

II. TIME-DEPENDENT DENSITY-FUNCTIONAL THEORY

We shall briefly summarize time-dependent density-functional theory, which forms the basis of our electronic quantum-mechanical calculations. In what follows we use atomic units (a.u.), so that with m_e denoting the electron mass and e its charge, length is given in units of the Bohr radius $a_0=\hbar^2/m_e e^2=0.529$ Å, energy in units of 1 hartree$=e^2/a_0=27.2$ eV, and time in units of $\hbar/1$ hartree$=2.42\times10^{-17}$ s.

In the derivation of the TDDF theory,[3] which can be considered an extension to time-dependent systems of the more familiar ground-state theory, it is first shown that the equations of motion of a system of N_e interacting electrons can be entirely formulated in terms of the space

and time-dependent density $n(\mathbf{x},t)$, instead of the more complex many-body wave function $\Phi(\mathbf{x}_1,\mathbf{x}_2,\ldots,\mathbf{x}_{N_e},t)$. A reference system of noninteracting fermions, with the same density as the interacting electron system, is then introduced, and it is shown that one can write the equations of motion in terms of a set of orthonormal, single-particle, time-dependent Kohn-Sham orbitals. The orbitals evolve according to the Schrödinger-like equations (keeping the variable $m_e=1$ explicit)

$$i\frac{\partial}{\partial t}\psi_j(\mathbf{x},t)=-\frac{1}{2m_e}\nabla^2\psi_j(\mathbf{x},t)+v_{\rm eff}(\mathbf{x},t[n])\psi_j(\mathbf{x},t)\ , \quad j=1,2,\ldots,N_e\ , \tag{1}$$

where the space- and time-dependent density $n(\mathbf{x},t)$ is given by

$$n(\mathbf{x},t)=\sum_{j=1}^{N_e}|\psi_j(\mathbf{x},t)|^2\ , \tag{2}$$

and where $v_{\rm eff}(\mathbf{x},t[n])$ is an effective potential with a self-consistent, functional dependence on the density. One can write

$$v_{\rm eff}(\mathbf{x},t[n])=v(\mathbf{x},t)+v_H(\mathbf{x},t)+\frac{\delta A_{\rm xc}}{\delta n(\mathbf{x},t)}\ , \tag{3}$$

where $v(\mathbf{x},t)$ is the potential due to the ions or to external forces, $v_H(\mathbf{x},t)$ the Hartree potential given by

$$v_H(\mathbf{x},t)=e^2\int d^3x'\frac{n(\mathbf{x}',t)}{|\mathbf{x}-\mathbf{x}'|}\ , \tag{4}$$

and where the exchange and correlation part of the action, $A_{\rm xc}=A_{\rm xc}[n]$, accounts for all other interaction effects.[3] Because Eqs. (1) provide an *exact* description of the interacting system, the task of finding the exact form of $A_{\rm xc}$ under all conditions is very difficult, as this term should account for exchange and correlation when the system is either in the ground state or at finite temperature, and should also be able to induce, through the mean field potential $v_{\rm eff}$, all of the relaxation processes which occur when the system is taken far from equilibrium.

Here, we adopt the simplest approximation for $A_{\rm xc}$, the so-called adiabatic, local-density approximation[10,11] (adiabatic LDA), in which one writes

$$A_{\rm xc}^{\rm LDA}[n]=\int_{t_0}^{t_1}dt\int d^3x\ n(\mathbf{x},t)\varepsilon_{\rm xc}(n(\mathbf{x}t))\ , \tag{5}$$

where $\varepsilon_{\rm xc}(n)$ is the exchange and correlation energy of a homogeneous electron gas of density n in the ground state. Equation (5) not only assumes locality in space, as in the LDA of ground-state density-functional theory, but also locality in time, and proximity to the ground state in the space of wave functions. This approximation is in fact sufficient if the scheme aims to achieve nothing more, within the approximation afforded by the ground-state LDA, than to adiabatically follow the instantaneous electronic ground-state energy surface (the so-called Born-Oppenheimer surface).[5,6]

III. EQUATIONS OF MOTION OF THE ELECTRON-ION SYSTEM

Equations (1) for the N_e valence electrons are coupled to Newton's equations for N_i classical ion cores, the effect of each of which is modeled by a local pseudopotential denoted by $v_{\rm ps}(\mathbf{x})$. For simplicity we assume unpolarized electrons, so that with double occupancy only $N_0=N_e/2$ time-dependent Kohn-Sham orbitals fully describe the electronic system. Here, we assume sodium ions, with mass M and valence charge $Z_v=1$, so that $N_e=N_i$. If the ionic positions at time t are given by $\{\mathbf{R}_k(t)\}$, $k=1,2,\ldots,N_i$, then the complete set of equations of motion is given by (keeping the variables $e=m_e=1$ explicit) (Ref. 5)

$$i\frac{\partial}{\partial t}\psi_j(\mathbf{x},t)=-\frac{1}{2m_e}\nabla^2\psi_j(\mathbf{x},t)+v_{\rm eff}(\mathbf{x},t,[n])\psi_j(\mathbf{x},t)\ , \quad j=1,2,\ldots,N_0=N_e/2\ , \tag{6}$$

$$M\frac{d^2}{dt^2}\mathbf{R}_k(t)=\mathbf{F}_k(t),\quad k=1,2,\ldots,N_i\ , \tag{7}$$

where $\mathbf{F}_k$ is the total force on the kth ion,

$$\mathbf{F}_k(t)=-\sum_l{}'\nabla_l\frac{e^2}{|\mathbf{R}_k(t)-\mathbf{R}_l(t)|}-\int d^3x\ v_{\rm ps}[\mathbf{x}-\mathbf{R}_k(t)]\nabla n(\mathbf{x},t)\ , \tag{8}$$

and where with double occupancy of orbitals the density is given by

$$n(\mathbf{x},t)=2\sum_{j=1}^{N_0}|\psi_j(\mathbf{x},t)|^2\ . \tag{9}$$

The effective potential can now be written

$$v_{\rm eff}(\mathbf{x},t,[n])=\sum_{k=1}^{N_i}v_{\rm ps}[\mathbf{x}-\mathbf{R}_k(t)]+v_H(\mathbf{x},t)+\mu_{\rm xc}(n(\mathbf{x},t))\ , \tag{10}$$

where the Hartree potential $v_H(\mathbf{x},t)$ is given by Eq. (4), and where the exchange and correlation term $\mu_{\rm xc}(n)$ is the local derivative

$$\mu_{\rm xc}(n)=\frac{d}{dn}[n\varepsilon_{\rm xc}(n)]\ , \tag{11}$$

where $\varepsilon_{\rm xc}(n)$ is given by the ground-state LDA.[12] Equations (6) and (7) can be derived from an action principle with the Lagrangian

$$L=2\int d^3x\sum_{j=1}^{N_0}\psi_j^*(\mathbf{x},t)\left[i\frac{\partial}{\partial t}+\frac{1}{2m_e}\nabla^2\right]\psi_j(\mathbf{x},t)-\tfrac{1}{2}\int d^3x\,d^3x'\frac{e^2}{|\mathbf{x}-\mathbf{x}'|}n(\mathbf{x},t)n(\mathbf{x}',t)$$
$$-\int d^3x\ n(\mathbf{x},t)\varepsilon_{\rm xc}(n(\mathbf{x},t))+\sum_k\tfrac{1}{2}M\left[\frac{d}{dt}\mathbf{R}_k(t)\right]^2-\sum_{k<l}\frac{e^2}{|\mathbf{R}_k(t)-\mathbf{R}_l(t)|}-\int d^3x\ n(\mathbf{x},t)\sum_{k=1}^{N_i}v_{\rm ps}[\mathbf{x}-\mathbf{R}_k(t)]\ . \tag{12}$$

The Lagrangian formulation is useful for deriving the conservation laws stated in Sec. III A.

The local sodium pseudopotential is taken to be of the form of Topp and Hopfield,[13]

$$v_{\rm ps}(r)=\begin{cases}0.1794[\cos(1.224r)-1], & 0\le r\le 3\\ -1/r, & 3<r\ ,\end{cases} \tag{13}$$

which is derived by fitting the predicted atomic energies to those of the ground state and first few excited states of the sodium atom. The pseudopotential defined by Eq. (13) is approximately norm conserving. The implementation of nonlocal pseudopotentials in the TDDF scheme is discussed in Appendix A.

It is important to emphasize that while Eqs. (6) and (7) assume classical ions, they are not a consequence of the Born-Oppenheimer approximation, because they allow for time-dependent, excited electronic states and for transitions between these states. Thus the electronic system is not tied to a ground state corresponding to the instantaneous ion positions, as would be required in the Born-Oppenheimer approximation. Equations (6) and (7) are in fact very similar in nature to the "classical-quantal" model of Schafer, Garcia, and Kwong[14] or to the time-dependent Hartree-Fock approach of Tiszauer and Kulander.[15] In our model, the Born-Oppenheimer approximation is realized only if system parameters are such that electron response to ion motion is adiabatic, and the initial electronic configuration is chosen to be the instantaneous ground state.

A. Conserved quantities

The equations of motion (6)–(11) imply three basic conservation relations. First, because Eq. (6) defines a set of Schrödinger-like equations for the wave functions, with identical potentials $v_{\rm eff}$, it follows from the unitary nature of the resulting evolution that orthonormality between wave functions is automatically conserved, with for all pairs (i,j) of orbitals

$$\int d^3x\ \psi_i^*(\mathbf{x},t)\psi_j(\mathbf{x},t)=\text{const}=\delta_{ij}\ . \tag{14}$$

Equation (14) affords the important simplification that orthogonality constraints need not be explicitly imposed on the equations of motion.[7] Equation (14) also ensures conservation of the total number of electrons, $dN(t)/dt=0$, where

$$N(t)=\int d^3x\ n(\mathbf{x},t)=N_e\ . \tag{15}$$

Second, the total momentum of the coupled electron-ion system is conserved, with $d\mathbf{P}(t)/dt=0$, where

$$\mathbf{P}(t)=\sum_l M\frac{d}{dt}\mathbf{R}_l(t)+2\sum_{i=1}^{N_0}\int d^3x\ \psi_i^*(\mathbf{x},t)(-i\nabla)\psi_i(\mathbf{x},t)\ . \tag{16}$$

Finally, the total energy is conserved, $dE(t)/dt=0$, where

$$E(t)=2\int d^3x\sum_i\psi_j^*(\mathbf{x},t)\left[-\frac{1}{2m_e}\nabla^2\right]\psi_j(\mathbf{x},t)+\tfrac{1}{2}\int d^3x\,d^3x'\frac{e^2}{|\mathbf{x}-\mathbf{x}'|}n(\mathbf{x},t)n(\mathbf{x}',t)$$
$$+\int d^3x\ n(\mathbf{x},t)\varepsilon_{\rm xc}(n(\mathbf{x},t))+\sum_k\tfrac{1}{2}M\left[\frac{d}{dt}\mathbf{R}_k(t)\right]^2+\sum_{k<l}\frac{e^2}{|\mathbf{R}_k(t)-\mathbf{R}_l(t)|}+\int d^3x\ n(\mathbf{x},t)\sum_{k=1}^{N_i}v_{\rm ps}[\mathbf{x}-\mathbf{R}_k(t)]\ . \tag{17}$$

We label the energy terms in Eq. (17), respectively, as follows:

$$E(t)\equiv E_{\rm EKE}+E_H+E_{\rm xc}+E_{\rm IKE}+E_{ii}+E_{ei}\ , \tag{18}$$

where $E_{\rm EKE}$ is the electron kinetic energy of the Kohn-Sham orbitals, which is the kinetic energy of the noninteracting reference system, E_H the electron Hartree energy, $E_{\rm xc}$ the electron exchange and correlation energy, $E_{\rm IKE}$ the ion kinetic energy, E_{ii} the ion potential energy due to ion-ion interaction, and finally E_{ei}, the electron-ion interaction energy. As usual, $E_{\rm EKE}$ contains only part of the kinetic energy of the interacting electrons, the remainder being implicitly accounted for in E_H and $E_{\rm xc}$. It should be emphasized that Eq. (17) does not contain the "fictitious" electronic kinetic energy term which is essential to the formulation of the Car-Parrinello method.[2]

B. Addition of a thermostat to the ionic equations of motion

The finite-temperature simulations are subject to an irreversible and unphysical flow of energy from the ions to the electrons, which is a consequence of the quantum-classical nature of the model, and which will be discussed in some detail in Sec. VI. As in Ref. 16, we resort to thermostatting the ions by the Nosé method,[17,18] and periodically quenching the electrons back to the instantaneous ground state by steepest-descent minimization. We use the thermostat formulation of Hoover,[19] which results in a more transparent form of the equations of motion than in Nosé's original derivation. Thus, through the introduction of new variables $\zeta(t)$ and $s(t)$, Eq. (7) is modified to read

$$M\frac{d^2}{dt^2}\mathbf{R}_k(t)=\mathbf{F}_k(t)-\zeta(t)M\frac{d}{dt}\mathbf{R}_k(t)\ ,\qquad k=1,2,\ldots,N_i\ , \tag{19}$$

to which are added the reservoir equations of motion

$$Q\frac{d}{dt}\zeta(t)=\sum_{k=1}^{N_i} M(\dot{\mathbf{R}}_k)^2-3N_i k_B T_{\rm res} , \tag{20}$$

$$\frac{d}{dt}\ln s(t)=\zeta(t) , \tag{21}$$

where $T_{\rm res}$ is the reservoir temperature and $\zeta(t)$ is a time-dependent dynamical friction (an effective collision frequency, which may be positive or negative) which couples the ionic system to the reservoir, of dynamical mass Q. The reservoir is represented by the single generalized coordinate $s(t)$, determined by integration of Eq. (21). Within the extended, microcanonical system represented by Eqs. (19)–(21), the ionic subsystem behaves as if part of a canonical ensemble at temperature $T_{\rm res}$. In thermal equilibrium, $\zeta(t)$ assumes values according to the probability distribution[19]

$$P(\zeta)=\left[\frac{Q}{2\pi k_B T_{\rm res}}\right]^{1/2}\exp(-Q\zeta^2/2k_B T_{\rm res}) , \tag{22}$$

and the characteristic oscillation frequency ω_ζ of $\zeta(t)$ is found to be

$$\omega_\zeta=(3N_i k_B T_{\rm res}/Q)^{1/2} . \tag{23}$$

In general, one chooses the dynamical mass Q so that $\omega_\zeta\sim\omega_{\rm ion}$, where $\omega_{\rm ion}$ is a typical frequency of the ionic system.[18] To start the simulations, we choose $\zeta(0)$ at random from the distribution of Eq. (22), and set $s(0)=1$.

With the modifications implied by Eqs. (19)–(21), it is now the total energy of the *extended* system,

$$E_{\rm tot}(t)=E(t)+\tfrac{1}{2}Q\zeta^2(t)+3N_i k_B T_{\rm res}\ln s(t) , \tag{24}$$

where $E(t)$ is the energy of the electron-ion system [Eq. (18)], which is a constant of the motion, and which thus provides a check on the accuracy of the numerical integration schemes.

IV. METHOD OF SOLUTION

In order to numerically solve Eqs. (6) and (19)–(21) we use a scheme in which the wave functions $\psi_j(\mathbf{x},t^n)$, the ionic positions $\{\mathbf{R}_k(t^n)\}$, and the dynamical friction $\zeta(t^n)$ are defined at integral times $t^n=n\Delta t$, $n=0,1,2,\ldots$, while the ionic velocities $\{\mathbf{v}_k(t^{n+1/2})\}$ and reservoir coordinate $s(t^{n+1/2})$ are defined at the midpoints $t^{n+1/2}=(n+1/2)\Delta t$. Given all data at $t=t^n$, the ions are moved according to the time-centered scheme

$$\mathbf{v}_k(t^{n+1/2})=\left[\frac{1-\Delta t\zeta(t^n)/2}{1+\Delta t\zeta(t^n)/2}\right]\mathbf{v}_k(t^{n-1/2}) +\frac{1}{1+\Delta t\zeta(t^n)/2}\frac{\Delta t}{M}\mathbf{F}_k(t^n) , \tag{25}$$

$$\mathbf{R}_k(t^{n+1})=\mathbf{R}_k(t^{n-1})+\Delta t\mathbf{v}_k(t^{n+1/2}) , \tag{26}$$

for $k=1,2,\ldots,N_i$, while the dynamical friction $\zeta(t)$ and the auxiliary variable $\xi(t)\equiv\ln s(t)$ are evolved according to

$$\zeta(t^{n+1})=\zeta(t^n)+\frac{\Delta t}{Q}\left[\sum_{k=1}^{N_i} M[\mathbf{v}_k(t^{n+1/2})]^2-3N_i k_B T_{\rm res}\right] , \tag{27}$$

$$\xi(t^{n+1/2})=\xi(t^{n-1/2})+\Delta t\zeta(t^n) . \tag{28}$$

The reservoir coordinate is at all times given by $s(t^{n+1/2})=\exp[\xi(t^{n+1/2})]$. In Eq. (25) the force on the kth ion is explicitly given by

$$\mathbf{F}_k(t^n)=-\sum_l{}'\frac{e^2}{|\mathbf{R}_k(t^n)-\mathbf{R}_l(t^n)|} -\int d^3x\, v_{\rm ps}[\mathbf{x}-\mathbf{R}_k(t^n)]\nabla n(\mathbf{x},t^n) . \tag{29}$$

Equations (25) and (28) are order Δt^3 accurate. In the absence of the thermostat, they reduce to the familiar Verlet algorithm[20]

$$\mathbf{v}_k(t^{n+1/2})=\mathbf{v}_k(t^{n-1/2})+\frac{\Delta t}{M}\mathbf{F}_k(t^n) , \tag{30}$$

$$\mathbf{R}_k(t^{n+1})=\mathbf{R}_k(t^{n-1})+\Delta t\mathbf{v}_k(t^{n+1/2}) , \tag{31}$$

for $k=1,2,\ldots,N_i$.

We assume a cubelike simulation region with periodic boundary conditions in all directions. In Eq. (29), the ion-ion force terms are evaluated from a tabulated high-order fit to the Ewald potential sum, while the electron-ion force term is computed using a fast Fourier transformation (FFT) to evaluate the integral sum in Fourier space.

We now consider the numerical integration of the Schrödinger equations given by Eq. (6). The effective potential occurring in the equations is straightforwardly determined from Eq. (10), where the Hartree term is most easily found from Poisson's equation,

$$\nabla^2 v_H(\mathbf{x},t)=-4\pi e^2 n(\mathbf{x},t) , \tag{32}$$

solved using a FFT method.

To evolve the wave functions according to Eq. (6), we must account for the nonlinearity implicit in the functional dependence $v_{\rm eff}=v_{\rm eff}[n]$. To maintain order Δt^3 accuracy in the presence of nonlinearity, we use a two-step Runge-Kutta scheme, in which we first obtain an approximation to the value of $v_{\rm eff}(t_n+\Delta t/2)$ by evolving all the wave functions through a half step, and using as an effective potential the already known value of $v_{\rm eff}(t^n)$. We then proceed with the full step by evolving all the wave functions from t^n to $t^n+\Delta t$, using for $v_{\rm eff}$ the approximation to $v_{\rm eff}(t_n+\Delta t/2)$ obtained from the half step.

With a given value of $v_{\rm eff}$, the actual solution of the Schrödinger equation is accomplished with a split-step method[21,22] combined with fast Fourier transforms. For instance, for the full step we use the decomposition

$$\psi_j(\mathbf{x},t^{n+1})=\exp\left[-i\frac{\Delta t}{2}v_{\text{eff}}(\mathbf{x},t^{n+1/2})\right]\times\exp[-i\Delta t(-\nabla^2/2m_e)]\times\exp\left[-i\frac{\Delta t}{2}v_{\text{eff}}(\mathbf{x},t^{n+1/2})\right]\psi_j(\mathbf{x},t^n) \quad (33)$$

and similarly for the preceding half step. The effect of the operator $\exp[-i\Delta t(-\nabla^2/2m_e)]$ is computed using three-dimensional fast Fourier transformations, while the effect of $\exp[-i(\Delta t/2)v_{\text{eff}}(\mathbf{x},t^{n+1/2})]$ is found from direct multiplication in real space. A total of four three-dimensional FFT's are needed per complete time step, two for the extrapolating half step, and two for the final full step. For a fixed physical evolution time the scheme is $O(\Delta t^2)$ accurate, and the overall speed of execution is almost proportional to the speed of execution of the individual three-dimensional FFT. Because of the real-space evaluation of the nonlinear terms such as v_{eff} or the exponential operators $\exp[-i(\Delta t/2)v_{\text{eff}}]$, the scheme embodied in Eq. (33) can be considered of the "pseudospectral" type.[23]

Because Eq. (33) is explicitly unitary, it conserves norm and orthogonality to roundoff. On the other hand, momentum and energy are not exactly conserved by Eqs. (25)–(29) and (33), and thus the changes of total energy and momentum over time provide a check on the accuracy of the overall scheme. In Appendix B we discuss the accuracy of Eq. (33) in more detail.

V. SIMULATION RESULTS

A. Numerical parameters

We have performed simulations of a system of 54 sodium ions and 54 valence electrons under periodic boundary conditions, at the density of the liquid at freezing ($\rho=0.932$ g cm^{-3}, $T_m=371$ K). The ion-sphere radius was $r_s=4.05$, and the simulation region was a cubical box with side $L=13.06$ Å. The electronic wave functions were defined on a grid $n_x\times n_y\times n_z=25\times25\times25$, with a maximum energy resolution of 5.50 hartree, and strictly periodic boundary conditions were imposed, so that the electronic states were only sampled at the Γ point. The ion-electron interaction was modeled by the local pseudopotential given by Eq. (13). In all cases the ions were initialized at the positions of the bcc solid, with 27 two-ion unit cells occupying the simulation box, and the electronic wave functions were initialized in a "Fermi cube" of 27 plane waves. With the ions fixed, the electronic energy was then minimized by a steepest-descent method.[2] The simulations were started by assigning the ions random velocities chosen from a Maxwellian distribution and temperature was maintained by the application of the Nosé thermostat. The value of the time step was $\Delta t=0.2$ a.u.

Evolving Eqs. (6) and (7) with the physical sodium ion mass $M=422\,280m_e$ is not feasible, because of the extreme disparity in electronic and ionic time scales which results. We drastically reduce the ion mass to a simulation value $M_{\text{sim}}=10m_e$, a procedure well known in the field of plasma simulation:[24] while much smaller than the real ion mass, M_{sim} is nonetheless large enough to ensure approximate adiabaticity of electron motion in response to the ionic displacements. Physical ionic frequencies ω are recovered by the extrapolation formula $\omega=(M_{\text{num}}/M)^{1/2}\omega_{\text{sim}}$, where ω_{sim} denotes the simulation result, and, with rescaling, each time step Δt is equivalent to 3.14×10^{-16} s of physical time. A formally equivalent approach to rescaling the ion mass is to rescale time in the one-particle Schrödinger equations; this approach is briefly discussed in Appendix C.

The computer simulations presented typically span 10^4 time steps, for an elapsed physical time of about 3.1 ps. For the system of 54 sodium ions, integration of a single time step requires 3 s of CPU time on a single processor of a Cray-2 computer, with 90% of execution time spent in three-dimensional fast Fourier transformations.

The electron wave functions are quenched to the instantaneous ground state by steepest descent every 200 time steps, corresponding to an elapsed time of 0.06 ps between quenches. The energy which is removed from the electronic system at each minimization, and which was gradually transferred from the ionic system over the preceding 200 time steps, is always less than 10% of the total ionic kinetic energy. For instance, in a simulation with ion temperature $T=325$ K, the maximum-energy electrons remain at all times within 2 meV ($=20\text{ K}\times k_B$) of the Born-Oppenheimer surface. In the absence of minimization, excellent energy and momentum conservation are observed in all cases, indicative of accurate integration of the equations of motion. For instance, at $T=10$ K, the average total electronic energy was of order 3.7 hartree, the average ionic kinetic energy of order 2×10^{-3} hartree, while the *total* energy of the coupled system was conserved to within 2×10^{-5} hartree over 10^4 time steps.

The present formulation assumes constant, nonfractional occupation of each time-dependent orbital, a constraint which can lead to error whenever a "level crossing" occurs, that is, whenever the energy gap between an occupied and an unoccupied state goes to zero on account of the finite ion displacements. However, we believe that the frequent quenches keep the electronic system sufficiently close to the Born-Oppenheimer surface at all times so that level crossings, when they do occur, introduce only minimal errors in the ion dynamics.

B. Ground-state calculations

We first performed calculations with no ion motion ($T=0$ K), and varied the volume so as to minimize the total ground-state energy of the system, thereby establishing the zero-temperature, zero-pressure equilibrium of bcc sodium. The results for the ion-sphere radius, binding energy per ion, and bulk modulus at equilibrium, shown in Table I, are in fair agreement with experiment.[25]

TABLE I. Equilibrium ($T=0$ K) results for the bcc sodium lattice (experimental results quoted in Ref. 22).

Quantity	Simulation	Experiment	% error
r_s at equilibrium	3.985	3.93	1.4
Binding energy/ion (hartree)	−0.228	−0.2305	1.1
Bulk modulus (kbar)	69.54	76	8.5

C. Radial distribution functions

We now consider results at finite temperature. The ion-ion radial distribution functions $g(r)$ for $T=325$ and 373 K are shown in Fig. 1. For $T=325$ K, although the system is in the solid phase, the trough between the second and third peaks of $g(r)$ is partially filled in and the radial distribution function strongly resembles that of a liquid. Indeed, for $T=373$ K the crystal has melted (Sec. V E), but the radial distribution function is only slightly less peaked than at $T=325$ K, confirming that no qualitative change in the shape of $g(r)$ intervenes across the phase boundary.

In Fig. 1 we also display experimental data for $T=378.5$ K (Ref. 26), which we compare to the $T=373$ K simulation results (neglecting the 1.5% difference in temperature). The simulation correctly predicts the positions of the foot, peak, and first trough of $g(r)$ ($r=5.3a_0$, $7a_0$, and $10a_0$, respectively), but overestimates the height of the peak by about 15% and the depth of the trough by about 10%. Factors which can account for this discrepancy are the small system size, and the short running time of the simulation (2.8 ps of elapsed physical time), both of which exaggerate the correlation between particles, and hence the height of oscillations in $g(r)$.

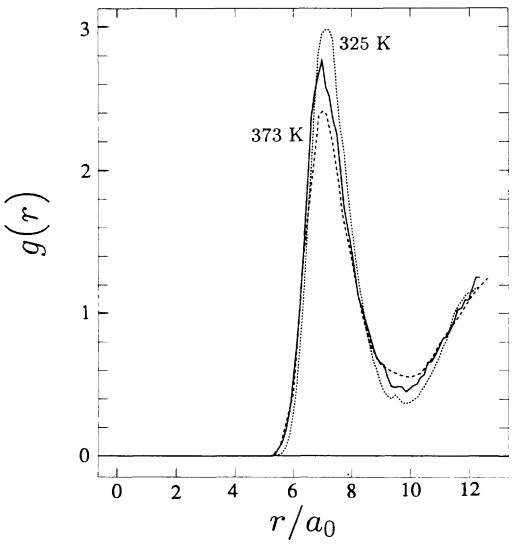

FIG. 1. Sodium ion-ion radial distribution functions obtained for $T=325$ (dotted line, topmost maximum) and 373 K (full line), compared to the experimental results for 378.5 K (Ref. 26, dashed line, lowest maximum).

D. Analysis of ion motion and of the phonon spectrum

In Fig. 2, we display for $T=10$ K the velocity autocorrelation function $Z(t)$, defined by[27]

$$Z(t)=\tfrac{1}{3}\langle \mathbf{v}(0)\cdot\mathbf{v}(t)\rangle \ . \tag{34}$$

In Eq. (34) $\mathbf{v}(t)$ denotes the time-dependent velocity of each ion and $\langle\ \rangle$ the ensemble average over all ion trajectories, which in the numerical simulation is replaced by a time average over all trajectories. The velocity autocorrelation functions were constructed from data accumulated over 8 ps, after an equilibration period of 1000 time steps, corresponding to an elapsed time of 0.31 ps.

As expected at low temperature, inspection of Fig. 2 shows that ion motion is a superposition of several frequencies due to the thermal excitation of phonons in the crystal lattice, with a comparatively long autocorrelation time.[28] A quantitative measure of the frequency content of the ion motion is given by the power spectrum $\hat{Z}(\omega)$, defined as the Fourier transform of $Z(t)$,

$$\hat{Z}(\omega)=\int_{-\infty}^{\infty} dt\, e^{i\omega t}Z(t) \ . \tag{35}$$

The power spectrum obtained from the simulation data is displayed in Fig. 3 where it is compared to the physically expected result, $\hat{Z}^{\rm phys}(\omega)$. In the harmonic approximation and in thermal equilibrium

$$\hat{Z}^{\rm phys}(\omega)=\frac{\pi v_0 k_B T}{3M}g(\omega) \ , \tag{36}$$

where v_0 is the volume of the bcc primitive unit cell and where $g(\omega)$ is the phonon density of modes,

$$g(\omega)=\frac{1}{V}\sum_{\mathbf{k},\sigma}\delta(\omega-\omega_{\mathbf{k},\sigma}^{\rm expt}) \ , \tag{37}$$

where $\omega_{\mathbf{k},\sigma}^{\rm expt}$ is the experimentally determined phonon frequency for wave vector $\mathbf{k}$ and polarization σ. Because of the small size of the simulation region, and the symmetry of the bcc lattice, only seven nonequivalent wave vectors within the first Brillouin zone give rise to distinct longitudinal and transverse nonzero frequencies, of which fur-

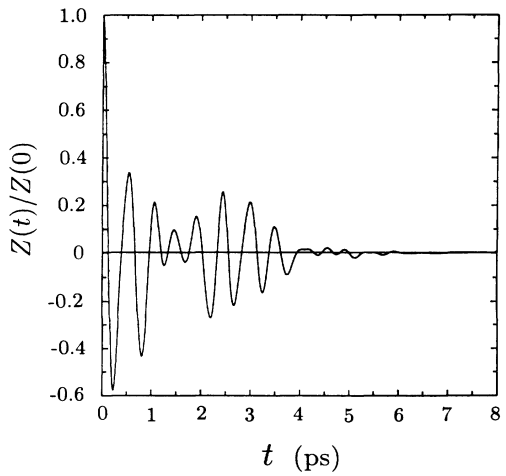

FIG. 2. Ion velocity autocorrelation function for $T=10$ K.

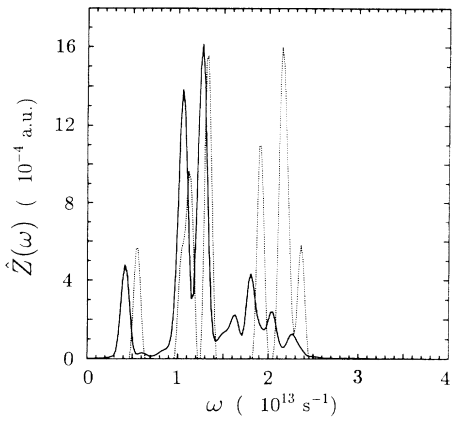

FIG. 3. Ion velocity power spectrum (full line) for $T=10$ K (this is the Fourier transform of the ion velocity autocorrelation function shown in Fig. 6). The dashed line shows the result expected on the basis of experimental data, $\hat{Z}^{\text{phys}}(\omega)$.

thermore only 13 are distinct. Thus Eq. (37) can be written with 13 distinct terms $\delta(\omega-\omega_{\mathbf{k},\sigma}^{\text{expt}})$, with appropriate weightings to account for degeneracies. The frequencies $\omega_{\mathbf{k},\sigma}^{\text{expt}}$ are obtained from the experimental data of Ref. 29. To account for the finite observation time over which the spectra are constructed, we replace $g(\omega)$, as given by Eq. (37), by its convolution with a window of finite width $\Delta\omega\sim\pi/t_{\text{lag}}$, where $t_{\text{lag}}=8$ ps is the maximum lag over which $Z(t)$ has been determined.

Inspection of Fig. 3 shows that $\hat{Z}(\omega)$ is qualitatively similar to $\hat{Z}^{\text{phys}}(\omega)$, with several peaks in the frequency range $0<\omega<2.5\times10^{13}$ s^{-1}. Nonetheless, the simulation predicts peaks at frequencies consistently lower than occurring in $\hat{Z}^{\text{phys}}(\omega)$, and a spurious peak at $\omega=1.6\times10^{13}$ s^{-1}. Furthermore, the high-frequency peaks in the range $1.5\times10^{13}<\omega<2.5\times10^{13}$ s^{-1} are of smaller amplitude than expected from comparison with $\hat{Z}^{\text{phys}}(\omega)$. This latter feature is an indication that in the simulation thermal equipartition of energy has not occurred for the high-frequency modes. Indeed, failure to reach complete equipartition is a common occurrence in traditional non-*ab-initio* molecular-dynamics calculations for low temperatures, where there is not enough anharmonicity in the lattice vibrations to naturally promote equipartition.[28] This difficulty is exacerbated in the present case, on account of the relatively short time span accessible to the fully self-consistent, *ab initio* simulation. These observations suggest that in future work greater care be taken to ensure fast equilibration at low temperatures. In particular, a Langevin equation might be used in the place of the Nosé thermostat in the early equilibration phase: the Langevin scheme introduces high-frequency noise in the ion motion, which should promote equipartition of energy at all frequencies on a faster time scale.

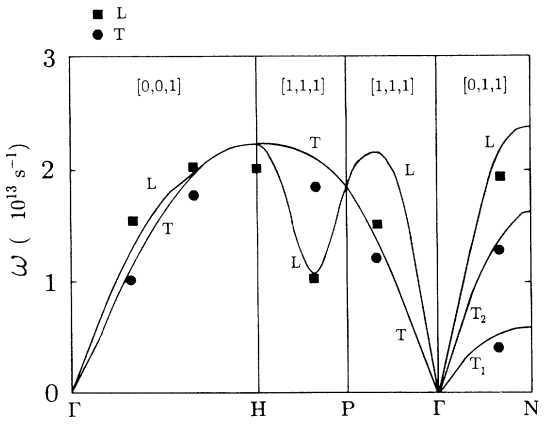

FIG. 4. Frequency dependence on wave vector in the bcc crystal lattice at $T=10$ K. Full lines: experimental results (Ref. 29); large dots: simulation results for the transverse modes; large squares: simulation results for the longitudinal modes. The large square at the H point denotes both the transverse and longitudinal mode frequencies.

To further resolve the frequency spectrum displayed in Fig. 3, we perform a mode-by-mode analysis of the ion motion.[28] For a given wave vector $\mathbf{k}$, we construct the Fourier-analyzed displacements $\hat{\mathbf{u}}(\mathbf{k},t)$, given by

$$\hat{\mathbf{u}}(\mathbf{k},t)=\sum_{j=1}^{N_i}[\mathbf{R}_j(t)-\mathbf{R}_j]\exp(-i\mathbf{k}\cdot\mathbf{R}_j)\ , \tag{38}$$

where the set of coordinates $\mathbf{R}_j=\mathbf{R}_j(0)$, $j=1,2,\ldots,$ refers to the initial bcc lattice positions. Spectral analysis of the autocorrelation functions $\langle\hat{\mathbf{u}}(\mathbf{k},t)\cdot\hat{\mathbf{u}}(\mathbf{k},0)\rangle$ then reveals the frequencies $\omega_{\mathbf{k},\sigma}$ for each wave vector $\mathbf{k}$ and polarizations $\sigma=1,2,3$. The results of this analysis are shown in Fig. 4, where we display frequency dependence on wave vector along several lines in the Brillouin zone, along with the experimentally determined dispersion curves.

We first consider the transverse modes (large dots). Starting from the Γ point in the Brillouin zone, it can be seen that while the shape of the dispersion curve is correct, the frequencies are consistently lower than the experimental values, with the maximum frequency at the H point underestimated by 9%. The predictions for the longitudinal mode frequencies (large squares) show roughly the same errors, with the exception of the $P\Gamma$ line, where the frequency of the mode with wave vector $(2\pi/3a)(1,1,1)$ is underestimated by 30%. This large error leads to the spurious peak seen in Fig. 3 at $\omega=1.6\times10^{13}$ s^{-1}. The errors recorded here are not too surprising in view of the known difficulties encountered in modeling alkali metals in the LDA.[30] Another factor possibly accounting for errors is the simple local pseudopotential used here, which might be replaced by a more accurate nonlocal form.[31]

In Fig. 5 we display $Z(t)$ for $T=325$ K. At this higher temperature, ion displacements are large and anharmonic effects are pronounced,[32] leading to a short phonon lifetime. The velocity autocorrelation function thus decays much faster than for $T=10$ K (note the much shorter horizontal scale). The resulting power spectrum, Fig. 6, shows that the sharp peaks of the $T=10$ K power spectrum have broadened and merged together. In addition, $\hat{Z}(\omega)$ exhibits a long tail extending well above the highest phonon frequency.

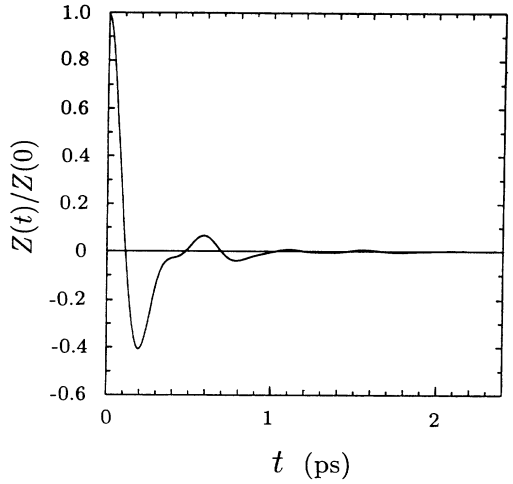

FIG. 5. Ion velocity autocorrelation function for $T=325$ K.

E. Prediction of the melting temperature

To estimate the onset of melting as a function of temperature, in Fig. 7 we display ion motion in the xy plane for an interval of 3 ps, at $T=10$, 100, 350, and 373 K. The density is fixed at $\rho=0.932$ g cm^{-3} ($r_s=4.05$), the experimental value for the liquid metal just above freezing. For $T=10$ K [Fig. 7(a)] ion excursions about the equilibrium positions are small as expected, becoming somewhat larger for $T=100$ K [Fig. 7(b)]. At $T=350$ K [Fig. 7(c)], displacements about the equilibrium positions are very large, at times extending halfway to the neighboring lattice sites, but remain strictly bounded. Finally, at $T=373$ K [Fig. 7(d)] ion motion is no longer bounded, and individual ions migrate to neighboring sites without returning to their initial positions. This results in a nonzero self-diffusion which we take as the signal that the crystal is melting.

To quantify the onset of self-diffusion and melting we compute the mean-square displacements of the ions as a function of time, with the definition

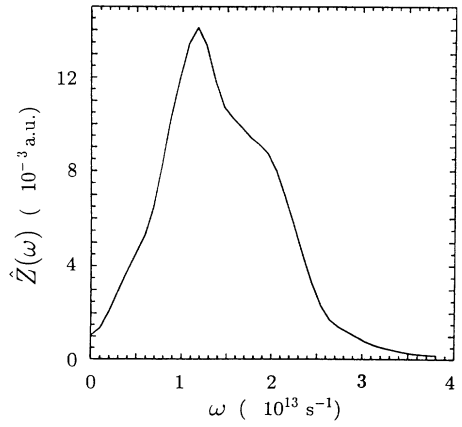

FIG. 6. Ion velocity power spectrum for $T=325$ K (this is the Fourier transform of the ion velocity autocorrelation function shown in Fig. 9).

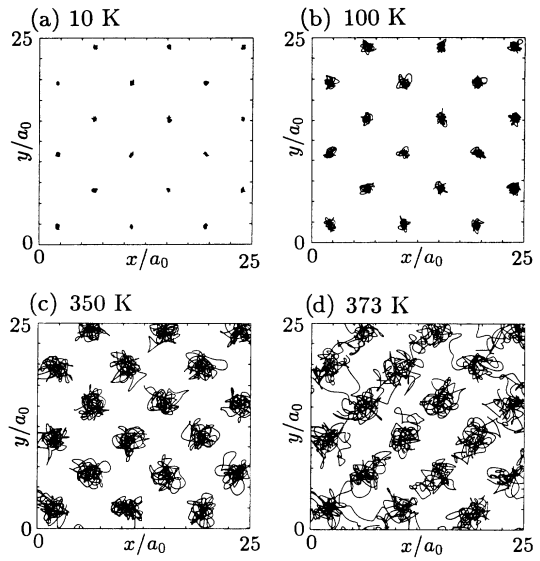

FIG. 7. Projection of ion orbits in the xy plane, for a duration of 3 ps starting from the bcc lattice configuration, at the temperatures indicated above each plot.

$$\langle \Delta \mathbf{r}^2(t) \rangle = \frac{1}{N_i} \sum_{j=1}^{N_i} [\mathbf{R}_j(t) - \mathbf{R}_j(0)]^2 \, . \tag{39}$$

The behavior of $\langle \Delta \mathbf{r}^2(t) \rangle$ for $T=350$, 360, 367, and 1000 K is shown in Fig. 8. The onset of unbounded ion motion, and hence of nonzero self-diffusion $D=\lim_{t\to\infty}\langle \Delta \mathbf{r}^2(t) \rangle /6t$, occurs in the range $350 \le T \le 360$ K (which we did not explore in greater detail due to limitations in computational resources). With

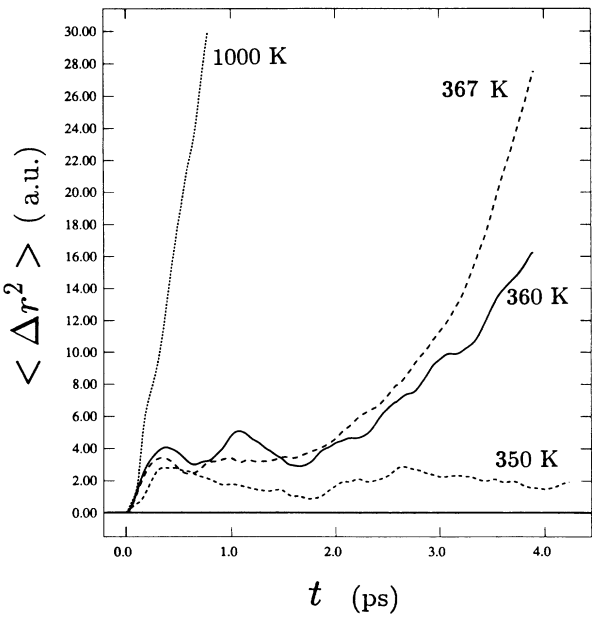

FIG. 8. Mean-square displacement of the ions as a function of time, for the temperatures indicated in the plot. The figure shows that the onset of self-diffusion occurs in the temperature range $350 < T < 360$ K.

this level of precision, the simulations thus predict a melting temperature T_m in the range $350 \leq T_m \leq 360$ K. As the experimental value is $T_m^{\text{expt}} = 371$ K, the error in the prediction is as large as 6%. The underestimation of the melting temperature is at least partly due to underestimation of the phonon frequencies (Figs. 3 and 4); at a given temperature this leads to an overestimation of ionic displacements, and, following the Lindemann criterion, to a lower threshold for melting of the crystal. Furthermore, the finite size of the simulation volume suppresses the longest wavelength modes and artificially raises the melting temperature,[33] so that in simulations on larger systems the error in the melting temperature will certainly increase, although it is hard to estimate the ultimate value of the error without actually performing these simulations. A more rigorous convergence study of the melting temperature, with both finer sampling of temperatures than in Fig. 8 and with simulations of larger numbers of ions is called for in future work.

Discussion of the behavior of the liquid metal has already been presented in Ref. 9, where it was shown that predictions of the self-diffusion coefficient are in reasonable agreement with experiment and comparable to those of previous work using the Car-Parrinello method.[8]

VI. DISCUSSION OF THE BREAKDOWN OF ADIABATICITY

In the course of the simulations the electron response to the ion motion is only approximately adiabatic. This is expected in a physical system, as electrons and ions can exchange energy through scattering mechanisms, leading to thermal equilibration, and as such does not contradict the assumptions leading to Eqs. (6) and (7). Starting with electrons in the instantaneous ground state, the physical consequence of nonadiabaticity should be a broadening of order $k_B T$ of the electron energy distribution about the Fermi energy, and a small concomitant transfer of energy from the ions to the electrons.

However, in the simulations the transfer of energy from the ionic to the electronic degrees of freedom has an irreversible component such that in the absence of a thermostat, and of periodic quenching of the electron wave functions, equilibration between electrons and ions is never achieved, even though total energy, as defined by Eq. (17), is rigorously conserved. A consequence of this irreversibility is the unphysical "cooling" of the ions at a rate increasing with initial ion temperature, which makes simulations at all but the lowest temperatures impractical unless one introduces the artifice of a thermostat and electronic quenches.

To illustrate this unphysical effect, in Fig. 9 we show the time evolution of the energy in simulations run without an ionic thermostat or periodic electronic quenching. In the left-hand column of the figure we display the evolution of the effective ion temperature T_I, defined as

$$T_I(t) \equiv \frac{2}{3N_i k_B} E_{\text{IKE}}(t) , \tag{40}$$

where E_{IKE} is the ion kinetic energy. We consider the initial conditions $T_I(0) = 200$, 1000, and 4000 K [Figs. 9(a), 9(b), and 9(c), respectively]. In all three cases, the ions start in the bcc crystal lattice configuration, so that the ion potential energy is initially at a minimum.

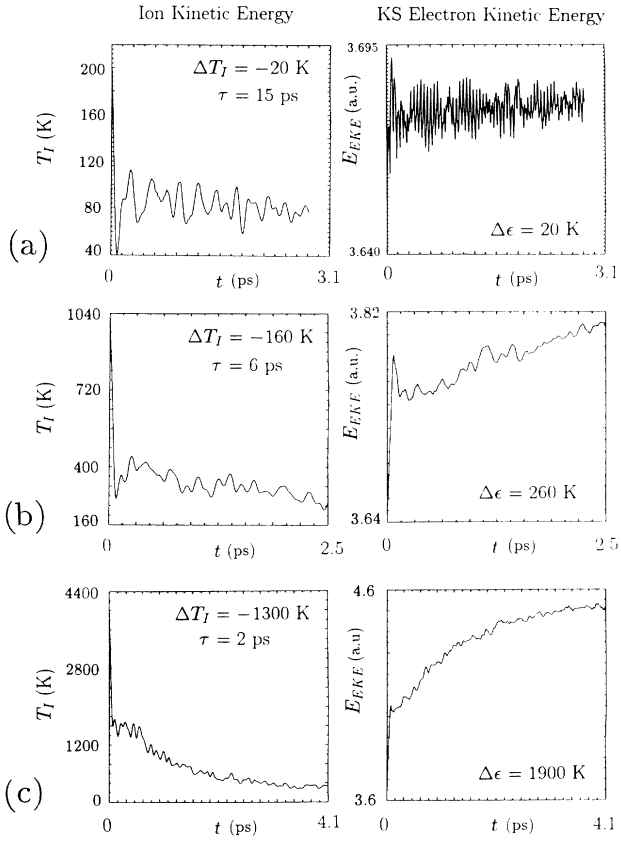

FIG. 9. Histories of the ion kinetic (left-hand column) and electron Kohn-Sham kinetic (right-hand column) energies for three different initial values of the effective ion temperature $T_I \equiv 2E_{\text{IKE}}/3N_i k_B$. Each row corresponds to a different initial temperature: (a) $T_I(0) = 200$ K, (b) $T_I(0) = 1000$ K, (c) $T_I(0) = 4000$ K. The drop $\Delta T_I(0)$ is a measure of ion energy loss, defined as the increment in $T_I(t)$, excluding the first 0.3 ps, and with fluctuations averaged over a sliding interval of 0.5 ps. The quantity $\Delta\varepsilon \equiv 2\Delta E_{\text{EKE}}/3N_i k_B$, displayed in the right-hand column, is a similar measure of the energy gain of the electrons.

For all initial conditions a short equilibrium phase first occurs, over the interval $0 \leq t \lesssim 0.3$ ps, during which the ion kinetic energy drops to about half its initial value. This phase is the result of approximate equipartition of energy between the kinetic and potential components of the total ion energy. For the remainder of each simulation the effective ion temperature then gradually decreases, over several picoseconds, on the time scales τ indicated in the figure. The total increment in effective temperature, ΔT_I, is also indicated in the figures. Because the total energy of the electron-ion system is conserved to high accuracy, the energy lost from the ionic system reappears in the electronic system. As a partial indication of this transfer of energy, we display the evolution of the Kohn-Sham electron kinetic energy E_{EKE} in the right-hand column of Fig. 9. A full account of energy

balance requires the display of the other energy terms E_{ii}, E_{ee}, and E_{ei} which appear in Eq. (18), but Fig. 9 suffices to indicate that the electrons are gaining energy to the detriment of the ions.

It should be emphasized that because the TDDF scheme embodies an approximation of the true electron dynamics, the mechanisms responsible for electron-ion energy transfer are physical processes. This is in strong contrast to the Car-Parrinello scheme where the electron orbitals evolve by virtue of a fictitious kinetic energy, and where energy transfer corresponds to an unphysical breakdown of adiabaticity.[34] In particular, in the TDDF scheme the dynamical linear response of the electronic system to perturbations includes not only the random phase approximation, but also local field corrections to the electron-electron interaction.[11] Furthermore, effects such as electron-phonon scattering in the solid, or Landau damping of sound waves in the liquid metal,[35] are present in the simulation. The presence in the TDDF scheme of these physical processes at first sight strongly suggests that electrons and ions should readily equilibrate, as in comparable but fully classical molecular-dynamics simulations of electron-ion systems.[24]

The failure of the electronic system to equilibrate with the ions is in fact due to a more fundamental limitation of the model, which occurs no matter how accurately the electronic system is simulated by itself: we believe it is a consequence of representing the ions by classical particles, while the electrons are modeled quantum mechanically. In such a "mixed" physical representation, thermal equilibrium between classical and quantum components is not possible, a situation which directly results from the suppression of spontaneous emission and for which we sketch a general argument in Appendix D, without pursuing the matter further in the present work.

The observation that the electron system cannot reach thermal equilibrium with the classical ions suggests that as in comparable Car-Parrinello simulations a numerical thermostat be coupled to the electronic system as well as the ions, replacing the periodic quenching procedure used here.[36,37] Whether such a procedure is practical will be the topic of future study.

VII. CONCLUSIONS

The TDDF scheme, based on Schrödinger-like equations for the evolution of the electronic wave functions, has been shown to give results comparable to those of the Car-Parrinello method when applied to sodium. With the implementation of nonlocal pseudopotentials, now under way, we expect that the TDDF scheme will be comparable to the Car-Parrinello method for a number of first-principles calculations, with the advantage of avoiding explicit orthonormality constraints in the electronic equations of motion. We have also shown that the difficulties associated with electron-ion equilibration when modeling metallic systems are of a different nature than those encountered with the Car-Parrinello method, and thus might be controlled by different means. Finally, the TDDF scheme holds the promise of applications in areas where the computation of electron dynamics is essential, such as the direct calculation of electronic transport in bulk materials,[22] or in electronic devices.[38] However, a full elucidation of the limitations of the quantum-classical model[39,40] will first have to be accomplished before such applications are routinely feasible.

ACKNOWLEDGMENTS

The author wishes to thank Professor S. Ichimaru for his hospitality and Professor S. Ichimaru, Dr. H. Iyetomi, and Dr. S. Ogata for stimulating exchanges during his stay at the University of Tokyo where part of this work was accomplished. Professor N. J. Fisch, Dr. R. Mendez, and Professor C. K. Birdsall are also cordially thanked for their support and for many discussions pertaining to this research. This work was performed under the auspices of the Japan Society for the Promotion of Science and the National Science Foundation, with partial support from the Institute for Supercomputing Research, Recruit Corporation, Tokyo. Computations were performed at the National Energy Research Supercomputing Center, Livermore, California, and at the San Diego Supercomputer Center.

APPENDIX A: IMPLEMENTATION OF NONLOCAL PSEUDOPOTENTIALS FOR THE ION CORES

We outline the steps in implementing nonlocal pseudopotentials in the TDDF scheme, including some of the difficulties we have so far encountered. Following Kleinman and Bylander[41] we model the ion cores by a combination of local and nonlocal pseudopotentials, with the local pseudopotential incorporating long-range effects. The total potential due to all the ions can be written

$$\hat{V}=\hat{V}_L+\hat{V}_{\rm NL}\ , \tag{A1}$$

where $\hat{V}_L$ and $\hat{V}_{\rm NL}$ are the sums of local and nonlocal pseudopotentials, respectively. The local term has the form (in coordinate representation)

$$\hat{V}_L(\mathbf{x})=\sum_{j=1}^{N_i} v_{\rm ps}(|\mathbf{x}-\mathbf{R}_j|)\ , \tag{A2}$$

where $v_{\rm ps}(r)$ is a spherically symmetric potential. The nonlocal term is given by

$$\hat{V}_{\rm NL}=\sum_{j=1}^{N_i}\sum_{l=0}^{l_{\max}}\sum_{m=-l}^{l}\frac{|v_l\phi_l;lm\rangle^{(j)}\langle v_l\phi_l;lm|^{(j)}}{\langle\phi_l|v_l|\phi_l\rangle}\ . \tag{A3}$$

In Eq. (A3),

$$\langle\mathbf{x}|v_l\phi_l;lm\rangle^{(j)}=\langle\mathbf{x}-\mathbf{R}_j|v_l\phi_l;lm\rangle^{(0)}\ , \tag{A4}$$

where the ket $|v_l\phi_l;lm\rangle^{(0)}$ refers to the state of an ion core at the origin,

$$\langle\mathbf{x}|v_l\phi_l;lm\rangle^{(0)}=v_l(r)\phi_l(r)Y_{lm}(\theta_{\mathbf{x}},\varphi_{\mathbf{x}})\ , \tag{A5}$$

where $v_l(r)$ is the radial dependence of the pseudopotential, and $\phi_l(r)$ the pseudowave function from which it was constructed. As a generalization of Eq. (33), we envisage

a split-step scheme of the form

$$\psi_j(t+\Delta t)=\exp\left[-i\frac{\Delta t}{2}v_{\text{eff}}\right]\exp\left[-i\frac{\Delta t}{2}\hat{V}_{\text{NL}}\right]$$
$$\times\exp[-i\Delta t(-\nabla^2/2m_e)]\exp\left[-i\frac{\Delta t}{2}\hat{V}_{\text{NL}}\right]$$
$$\times\exp\left[-i\frac{\Delta t}{2}v_{\text{eff}}\right]\psi_j(t)\ , \tag{A6}$$

where v_{eff} includes both the electron self-interaction terms, and the local part of the pseudopotentials, as in Eq. (10). The computational problem at hand is to implement the effect of the operator $\exp[-i(\Delta t/2)\hat{V}_{\text{NL}}]$.

We assume that for different ions the supports of nonlocal pseudopotentials do not intersect, so that for all values of $\mathbf{x}$ and l,l'

$$v_l(|\mathbf{x}-\mathbf{R}_j|)v_{l'}(|\mathbf{x}-\mathbf{R}_k|)=0 \quad \text{when } j\neq k\ . \tag{A7}$$

Equation (A7) obtains if the distance of closest approach of any two ions is never less than $2r_c$, where r_c is the radius over which the nonlocal pseudopotential is nonzero. With Eq. (A7) true, one straightforwardly obtains the expansion

$$\exp(-i\tau\hat{V}_{\text{NL}})=1+\sum_{j=1}^{N_i}\sum_{l=0}^{l_{\max}}\sum_{m=-l}^{l}\gamma_l|v_l\phi_l;lm\rangle^{(j)}\times\langle v_l\phi_l;lm|^{(j)}\ , \tag{A8}$$

where

$$\gamma_l=\frac{e^{-i\tau\beta_l}-1}{\langle v_l\phi_l|v_l\phi_l\rangle}\ , \tag{A9}$$

with

$$\beta_l=\frac{\langle v_l\phi_l|v_l\phi_l\rangle}{\langle\phi_l|v_l|\phi_l\rangle}\ . \tag{A10}$$

The expectation values in Eqs. (A9) and (A10) are given by

$$\langle\phi_l|v_l|\phi_l\rangle=4\pi\int_0^\infty dr\, r^2v_l(r)\phi_l^2(r)\ , \tag{A11}$$

$$\langle v_l\phi_l|v_l\phi_l\rangle=4\pi\int_0^\infty dr\, r^2v_l^2(r)\phi_l^2(r)\ . \tag{A12}$$

The transformation induced by Eq. (A8) is easiest to evaluate in Fourier space. Introducing a plane-wave basis $\{|\mathbf{q}\rangle\}$, such that

$$\langle\mathbf{x}|\mathbf{q}\rangle=\frac{1}{V^{1/2}}e^{i\mathbf{q}\cdot\mathbf{x}}\ , \tag{A13}$$

where V denotes the system volume, we find the matrix elements

$$\langle\mathbf{q}|\exp(-i\tau\hat{V}_{\text{NL}})|\mathbf{q}'\rangle=\delta_{\mathbf{q},\mathbf{q}'}+\frac{1}{V}\sum_{j=1}^{N_i}e^{-i(\mathbf{q}-\mathbf{q}')\cdot\mathbf{R}_j}\sum_{l=0}^{l_{\max}}\gamma_l\lambda_l(q)\lambda_l(q')P_l(\cos\theta_{\mathbf{q},\mathbf{q}'})\ , \tag{A14}$$

where $\theta_{\mathbf{q},\mathbf{q}'}$ denotes the angle between the vectors $\mathbf{q}$ and $\mathbf{q}'$, P_l the Legendre polynomial of degree l, and with

$$\lambda_l(q)=\sqrt{4\pi(2l+1)}\int_0^\infty dr\, r^2j_l(qr)v_l(r)\phi_l(r)\ . \tag{A15}$$

The matrix defined by Eq. (A14) is exactly unitary in the infinite-dimensional space spanned by $\{|\mathbf{q}\rangle\}$. In practice, the set of plane waves is finite, so that the matrix is truncated, and furthermore the integrals of Eq. (A15) are evaluated with finite numerical errors. The resulting transformation matrix will thus only be approximately unitary. This state of affairs introduces a complication in the implementation of Eq. (A6), as unitarity of the successive operators is crucial in maintaining orthonormality of the Kohn-Sham wave functions. Nonetheless, if high accuracy can be obtained in evaluating Eq. (A14) (say, of the same order as total energy conservation), the progressive loss of exact orthonormality at each time step might be tolerable, all the more so if, as in the present case, the wave functions are automatically reorthonormalized every few hundred time steps. To investigate these numerical issues we are currently implementing Eq. (A6) directly as outlined above.

APPENDIX B: ACCURACY OF THE SPLIT-STEP METHOD

As it is not widely available in the literature, an expression for the error term in the split-step method, Eq. (33), will be given. If we write the Hamiltonian for the single-particle wave equation as $H=T+V$ where $T=\mathbf{p}^2/2m_e$ and $V=v_{\text{eff}}(\mathbf{x})$, we can define an effective Hamiltonian H_{num}, which contains the numerical error terms, through the relation

$$\exp\left[-i\frac{\Delta t}{2}V\right]\exp(-i\Delta tT)\exp\left[-i\frac{\Delta t}{2}V\right]$$
$$\equiv\exp(-i\Delta tH_{\text{num}})\ . \tag{B1}$$

A straightforward expansion of both sides of Eq. (B1) then yields the expression

$$H_{\text{num}}=H+\frac{\Delta t^2}{24}C+O(\Delta t^4)\ , \tag{B2}$$

where $C=[2T-V,[T,V]]$. One has the decomposition

$$C=A+B\ , \tag{B3}$$

where

$$A=-[\nabla v_{\text{eff}}(\mathbf{x})]^2 \tag{B4}$$

and

$$B=-\tfrac{1}{2}\sum_{\mu,\nu=1}^{3}\left[p_\mu p_\nu\frac{\partial^2 v_{\text{eff}}}{\partial x_\mu \partial x_\nu}+2p_\mu\frac{\partial^2 v_{\text{eff}}}{\partial x_\mu \partial x_\nu}p_\nu+\frac{\partial^2 v_{\text{eff}}}{\partial x_\mu \partial x_\nu}p_\mu p_\nu\right], \tag{B5}$$

where in the coordinate representation $p_\mu=-i\partial/\partial x_\mu$. Equations (B4) and (B5) show that errors will principally arise from regions where the gradient or second derivatives of v_{eff} are large.

It is tempting to try to obtain $O(\Delta t^4)$ accuracy in the split-step scheme, by absorbing as much as possible of the error terms into the definition of v_{eff} itself. For instance, the replacement

$$v_{\text{eff}}\rightarrow v_{\text{eff}}+\frac{\Delta t^2}{24}[\nabla v_{\text{eff}}(\mathbf{x})]^2 \tag{B6}$$

nullifies the error term A in Eq. (B3). Indeed, in equilibrium, imaginary-time calculations where one evaluates the propagator with the replacement $\Delta t\rightarrow -i\Delta\tau$, with τ a real number, the substitution of Eq. (B6) is enough to obtain effective $O(\Delta\tau^4)$ precision,[42] because the contributions of the remaining error term B, while nonzero at each time step, exactly sum to zero under the quantum-mechanical trace used to construct the equilibrium expectation values. In the present real-time calculation, there is no equivalent cancellation, and no obvious way to nullify the effects of B through a substitution equivalent to Eq. (B6). This is because B contains mixed coordinate and momentum operators, while the split-step method depends for its implementation on a strict separation of these operators in the terms V and T of Eq. (B1). Numerical experiments with Eq. (B6) alone have not yielded measurable improvements in accuracy, and have not been pursued here.

Higher-order split-step schemes, with more than three terms in the decomposition of the evolution operator, and $O(\Delta t^5)$ accuracy at each time step are available.[43] However, the tradeoff between higher accuracy per time step, and considerably greater algorithmic complexity and execution time per step, is not immediately clear. For this reason, implementation of such a higher-order scheme has not been attempted here.

An alternative method for integrating the time-dependent Schrödinger equation which does not depend on a split-step decomposition is the so-called second-order differencing scheme[44,45] (SOD scheme), where one writes

$$\psi(t+\Delta t)=\psi(t-\Delta t)-2i\Delta t H\psi(t)\ . \tag{B7}$$

With appropriate definition of norms and scalar products, the transformation induced by Eq. (B7) is exactly unitary, and is $O(\Delta t^3)$ accurate. An advantage of this scheme over the split-step method is that the exact eigenstates of H are stationary under Eq. (B7), while in the split-step method only the eigenstates of H_{num} are stationary, leading to $O(\Delta t^2)$ errors in the energies. Disadvantages of the SOD scheme are that it requires two sets of three-dimensional arrays instead of one, has more stringent stability limits, and large time-evolution errors for large kinetic energies. The scheme has not been implemented in the present work.

APPENDIX C: RESCALING TIME IN THE ONE-PARTICLE SCHRÖDINGER EQUATIONS

The one-particle Schrödinger equations, Eqs. (6), can be modified to read

$$i\lambda\frac{\partial}{\partial t}\psi_j(\mathbf{x},t)=-\frac{1}{2m_e}\nabla^2\psi_j(\mathbf{x},t)+v_{\text{eff}}(\mathbf{x},t,[n])\psi_j(\mathbf{x},t)\ ,\quad j=1,2,\ldots,N_0=N_e/2\ , \tag{C1}$$

where λ is a purely numerical factor which artificially modifies the rate of evolution of the electron wave functions. If $\lambda\gg 1$, electronic evolution is greatly slowed down, and a larger time step can be taken to integrate the equations of motion. The introduction of λ is justified if one is evolving the electrons assuming the instantaneous ground-state approximation, and provided that λ is not too large, so that approximate adiabaticity of electron motion is maintained. Defining a simulation time $\tau=t/\lambda$, the equations of motion take the form

$$i\frac{\partial}{\partial\tau}\psi_j(\mathbf{x},\tau)=-\frac{1}{2m_e}\nabla^2\psi_j(\mathbf{x},\tau)+v_{\text{eff}}(\mathbf{x},\tau,[n])\psi_j(\mathbf{x},\tau)\ ,\quad j=1,2,\ldots,N_0=N_e/2\ , \tag{C2}$$

$$M_{\text{sim}}\frac{d^2}{d\tau^2}\mathbf{R}_k(\tau)=\mathbf{F}_k(\tau),\quad k=1,2,\ldots,N_i\ , \tag{C3}$$

where the "simulation mass" M_{sim} is

$$M_{\text{sim}}=M/\lambda^2\ . \tag{C4}$$

With $\lambda>1$ Eqs. (C2) and (C3) are formally identical to simulating a system with artificially light ions, as is done in the present work.

APPENDIX D: QUANTUM-CLASSICAL EQUILIBRATION IN A TWO-LEVEL SYSTEM

We consider an idealized system composed of electrons bound in a two-level system, interacting with a heat reservoir of harmonic oscillators with a continuous distribution of frequencies. Let the excited- and ground-state energies of the electrons be E_a and E_b, respectively, with $E_a-E_b\equiv\hbar\Omega$, and the frequency distribution of the oscillators be $D(\omega)$. Following the analysis given in Ref. 46 of the evolution equation for the density matrix ρ of the electronic system, one obtains the coupled equations for the mean atomic level populations $N_a\equiv\rho_{aa}$ and $N_b\equiv\rho_{bb}$,

$$\frac{dN_a}{dt}=-\gamma[n(\Omega)+1]N_a+\gamma n(\Omega)N_b\ , \tag{D1}$$

$$\frac{dN_b}{dt}=\gamma[n(\Omega)+1]N_a-\gamma n(\Omega)N_b\ , \tag{D2}$$

where, with appropriate normalization of the linear coupling constant $g(\Omega)$, $\gamma=2\pi D(\Omega)g^2(\Omega)$ is the rate of spontaneous emission of the excited electrons (identical to the golden-rule expression), and where $n(\omega)$ is the mean number of harmonic-oscillator phonons in thermal equilibrium for an oscillator with frequency ω.

According to Eqs. (D1) and (D2), equilibrium $\dot{N}_a=\dot{N}_b=0$ is achieved when

$$N_a[n(\Omega)+1]=N_b n(\Omega)\ , \tag{D3}$$

in other words when the rate of spontaneous and induced emission from level a equals the rate of induced absorption from level b. With the distribution $n(\omega)=1/[\exp(\hbar\omega/k_BT)-1]$, Eq. (D3) then yields the correct Boltzmann distribution for the electronic system, $N_a/N_b=\exp(-\hbar\Omega/k_BT)=\exp[-(E_a-E_b)/k_BT]$.

Now, assume that the harmonic oscillators are from the outset assumed classical. The model is then modified in two ways, (1) spontaneous emission is suppressed, so that in Eqs. (D1) and (D2) one should replace the terms $N_a[n(\Omega)+1]$ by $N_a n(\Omega)$, and (2), the equilibrium phonon distribution is now the classical equipartition $n(\omega)=k_BT/\hbar\omega$. The equilibrium condition becomes

$$N_a n(\omega)=N_b n(\omega)\ , \tag{D4}$$

with the only possible solution $N_a=N_b$. Thus the atomic energy levels are equally populated in equilibrium, in complete contradiction to the correct Boltzmann distribution. This unphysical behavior directly follows from the suppression of spontaneous emission, in fact independently of the form of $n(\omega)$. It is important to emphasize that Eq. (D4) is not a high-temperature approximation to Eq. (D3), but is an *exact* relation, resulting from the assumption that the oscillators are exactly classical at *all* temperatures (as are the ions in the TDDF model presented here).

If an additional mechanism (such as another heat reservoir) is introduced to maintain a Boltzmann distribution $N_a/N_b=\exp[-(E_a-E_b)/k_BT]$ in the atomic system, then equilibration between the electrons and the oscillators still cannot occur, as Eq. (D4) cannot be satisfied for $N_a\neq N_b$. In this case, there will be a continuous and unphysical flux of energy from the harmonic oscillators to the electrons.

---

*Present address: Thinking Machines Corporation, 245 First Street, Cambridge, MA 02142.

[1]R. Car and M. Parrinello, Phys. Rev. Lett. **55**, 2471 (1985).
[2]D. K. Remler and P. A. Madden, Mol. Phys. **70**, 921 (1990).
[3]E. Runge and E. K. U. Gross, Phys. Rev. Lett. **52**, 997 (1984).
[4]G. W. Fernando, G.-X. Qian, M. Weinert, and J. W. Davenport, Phys. Rev. B **40**, 7985 (1989).
[5]E. Fois, A. Selloni, M. Parrinello, and R. Car, J. Phys. Chem. **92**, 3268 (1988).
[6]E. Fois, A. Selloni, and M. Parrinello, Phys. Rev. B **39**, 4812 (1989).
[7]R. Kalia, P. Vashishta, L. H. Yang, F. W. Deck, and J. Rowland, Int. J. Supercomputer Appl. **4**, 22 (1990).
[8]G.-X. Qian, M. Weinert, G. W. Fernando, and J. W. Davenport, Phys. Rev. Lett. **64**, 1146 (1990).
[9]J. Theilhaber, Phys. Fluids B **4**, 2044 (1992).
[10]A. Zangwill and P. Soven, Phys. Rev. A **21**, 1561 (1980).
[11]E. K. U. Gross and W. Kohn, in *Advances in Quantum Chemistry* (Academic, New York, 1990), Vol. 21, p. 255.
[12]J. P. Perdew and A. Zunger, Phys. Rev. B **23**, 5048 (1981).
[13]W. C. Topp and J. J. Hopfield, Phys. Rev. B **7**, 1295 (1973).
[14]K. J. Schafer, J. D. Garcia, and N.-H. Kwong, Phys. Rev. B **36**, 1872 (1987).
[15]D. Tiszauer and K. C. Kulander, Phys. Rev. A **29**, 2909 (1984).
[16]I. Stich, R. Car, and M. Parrinello, Phys. Rev. Lett. **63**, 2240 (1989).
[17]S. Nosé, Mol. Phys. **52**, 255 (1984).
[18]S. Nosé, J. Chem. Phys. **81**, 511 (1984).
[19]W. G. Hoover, Phys. Rev. A **31**, 1695 (1985).
[20]L. Verlet, Phys. Rev. **159**, 98 (1967).
[21]M. D. Feit, J. A. Fleck, and A. Steiger, J. Comput. Phys. **47**, 412 (1982).
[22]R. K. Kalia, P. Vashishta, and S. W. de Leeuw, J. Chem. Phys. **90**, 6802 (1989).
[23]C. A. J. Fletcher, *Computational Techniques for Fluid Dynamics* (Springer, Berlin, 1988), p. 151.
[24]C. K. Birdsall and A. B. Langdon, *Plasma Physics via Computer Simulation* (Hilger, New York, 1991).
[25]J. Hafner, *From Hamiltonian to Phase Diagrams: The Electronic and Statistical-Mechanical Theory of sp-bonded Metals and Alloys* (Springer, Berlin, 1987), p. 73.
[26]T. Iida and R. I. L. Guthrie, *The Physical Properties of Liquid Metals* (Clarendon, Oxford, 1988), p. 27.
[27]J.-P. Hansen and I. R. McDonald, *Theory of Simple Liquids*, 2nd ed. (Academic, London, 1986), p. 199.
[28]J. M. Dickey and A. Paskin, Phys. Rev. **188**, 1407 (1969).
[29]A. D. B. Woods, B. N. Brockhouse, R. H. March, A. T. Stewart, and R. Bowers, Phys. Rev. **128**, 1112 (1962).
[30]V. L. Moruzzi, J. F. Janak, and A. R. Williams, *Calculated Electronic Properties of Metals* (Pergamon, New York, 1978).
[31]U. Röthlisberger and W. Andreoni, J. Chem. Phys. **94**, 8129 (1991).
[32]N. H. March and M. Parrinello, *Collective Effects in Solids and Liquids* (Hilger, Bristol, 1982), p. 68.
[33]B. J. Alder and T. E. Wainwright, J. Chem. Phys. **31**, 459 (1959).
[34]G. Pastore, E. Smargiassi, and F. Buda, Phys. Rev. A **44**, 6334 (1991).
[35]D. Pines and P. Nozières, *The Theory of Quantum Liquids* (Addison-Wesley, Redwood City, 1989), p. 238.
[36]M. Grilli and E. Tosatti, Phys. Rev. Lett. **62**, 2889 (1989).
[37]P. E. Blöchl and M. Parrinello, Phys. Rev. B **45**, 9413 (1992).
[38]A. Nakano, P. Vashishta, and R. K. Kalia, Phys. Rev. B **43**, 9066 (1991).
[39]J. C. Tully, J. Chem. Phys. **93**, 1061 (1990).
[40]B. Space and D. F. Coker, J. Chem. Phys. **94**, 1976 (1992).
[41]L. Kleinman and D. M. Bylander, Phys. Rev. Lett. **48**, 1425

(1982).
[42]M. Takahashi and M. Imada, J. Phys. Soc. Jpn. **53**, 3765 (1984).
[43]C. H. Cooke and A. G. McMorran, J. Comput. Phys. **95**, 303 (1991).
[44]R. Kosloff and D. Kosloff, J. Chem. Phys. **79**, 1823 (1983).
[45]D. Kosloff and R. Kosloff, J. Comput. Phys. **52**, 35 (1983).
[46]M. Sargent III, M. O. Scully, and W. E. Lamb, Jr., *Laser Physics* (Addison-Wesley, Reading, MA, 1974), p. 276.